Neural ODE Approach to the Magnetic QCD Phase Diagram via Holography

Hong-An Zeng[a](To be evaluated), Rong-Gen Cai[b,c,d,e], Song He[a,b,c,f], Li Li[d,e,g]
[a] *Center for Theoretical Physics and College of Physics, Jilin University, Changchun 130012, People's Republic of China*
[b] *Institute of Fundamental Physics and Quantum Technology, Ningbo University, Ningbo, Zhejiang 315211, China*
[c] *School of Physical Science and Technology, Ningbo University, Ningbo, 315211, China*
[d] *CAS Key Laboratory of Theoretical Physics, Institute of Theoretical Physics, Chinese Academy of Sciences, Beijing 100190, China*
[e] *School of Fundamental Physics and Mathematical Sciences, Hangzhou Institute for Advanced Study, UCAS, Hangzhou 310024, China*
[f] *Max Planck Institute for Gravitational Physics (Albert Einstein Institute), Am Mühlenberg 1, 14476 Golm, Germany and*
[g] *School of Physical Sciences, University of Chinese Academy of Sciences, Beijing 100049, China.*[*]

We present a novel quantitative holographic QCD model incorporating neural ordinary differential equations (ODEs) to map the QCD phase diagram, including magnetic fields, baryon chemical potential, and temperature. This approach directly fits parameters to lattice QCD data, achieving strong agreement and revealing previously unexplored features, such as dual critical endpoints (CEPs) with non-mean-field critical exponents. Our framework provides new insights into the effects of magnetic fields on QCD, extending our understanding of strongly coupled systems and paving the way for experimental validation.

Introduction—Quantum Chromodynamics (QCD), the theory describing strong interactions, governs the behavior of quarks and gluons under extreme conditions and is central to understanding phenomena in high-energy physics, astrophysics, and cosmology. Studying the QCD phase diagram is essential for exploring the transition between the deconfined quark-gluon plasma and hadronic matter. This transition is particularly relevant to non-central heavy-ion collisions, neutron stars, and conditions in the early universe [1–3]. Significant efforts has been made to understand the equations of sate of QCD matter in the non-perturbative regime. It is now believed that, in the presence of magnetic field ($B = 0$), QCD undergoes a smooth thermal crossover at low baryon chemical potential μ_B by changing the temperature T, while there becomes a first-order transition at large μ_B. To search the critical endpoint (CEP) is a core objective for Heavy ion collisions. Moreover, magnetic fields play a crucial role in non-central heavy-ion collisions, where intense fields are generated, and magnetars, where the field strengths reach astronomical levels [4]. These fields significantly influence QCD matter, affecting the critical temperature of phase transitions, thereby establishing B as an essential factor in QCD studies.

However, exploring the complete QCD phase diagram at finite μ_B and B is challenging, particularly in the abovementioned environments. Lattice QCD calculations face the notorious sign problem at finite μ_B [2]. Moreover, simulating high-field configurations demands substantial computational resources [4]. Given these challenges and the lack of direct experimental evidence for the CEP, holographic methods offer a promising alternative for advancing our understanding of the QCD phase structure within a controllable non-perturbative framework. By mapping strongly coupled non-Abelian gauge theories into classical gravity dynamics, the holographic approach has shown promise in describing hot and dense QCD [6–8]. The most challenge is to determine the gravitational models using available lattice and experimental data. The bulk gravitational theory has a functional degree of freedom, known as the inverse problem. Exhaustively exploring all possible model parameters to fit the data is akin to searching for a needle in a haystack, for which manually tuning control parameters becomes impractical. Only few works [8, 12, 20] have tried incorporated magnetic fields in holographic models.

One the other hand, machine learning has become a powerful artificial intelligence technique in representing complex correlation. It can easily extract relevant features from complex data. Combination of machine learning and holography provides a data-driven gravity modeling of strongly coupled quantum systems. In this Letter, we introduce machine learning, specifically neural ordinary differential equations (ODEs), to optimize the complex parameter space of gravitational models, enabling a precise fit to lattice data and improving quantitative accuracy in capturing magnetic effects.

Unlike previous machine learning applications that rely on empirical formulas to fit finite-dimensional parameters [23–27], the novelty of our approach is to directly optimize the interaction forms over complex parameter spaces without semi-empirical guidance. We present the first fully quantitative three-dimensional QCD phase diagram. It not only confirms anticipated phase structures at $B = 0$ case and $\mu_B = 0$ case, but also reveals surprising novel features. In particular, it uncovers the existence of two CEPs in the T-μ_B plane under strong magnetic

fields, which could significantly impact future experimental research in high-energy physics.

Holographic model–To capture essential QCD dynamics at finite magnetic field, temperature, and baryon chemical potential, we employ a holographic framework based on the five-dimensional Einstein-Maxwell-Dilaton (EMD) theory:

$$S = \frac{1}{2\kappa_N^2}\int d^5x\sqrt{-g}\Big[\mathcal{R} - \frac{1}{2}\nabla_\mu\phi\nabla^\mu\phi - \frac{Z(\phi)}{4}F_{\mu\nu}F^{\mu\nu} - \frac{\hat{Z}(\phi)}{4}\hat{F}_{\mu\nu}\hat{F}^{\mu\nu} - V(\phi)\Big], \quad (1)$$

where κ_N^2 is the effective Newton constant. The metric $g_{\mu\nu}$ characterizes spacetime geometry, and the real scalar field ϕ accounts for conformal symmetry breaking. The Maxwell field A_μ with $F_{\mu\nu} = \partial_\mu A_\nu - \partial_\nu A_\mu$ introduces a finite baryon number density, while the magnetic field B is described by another Maxwell field $\hat{A}_\mu$ with $\hat{F}_{\mu\nu} = \partial_\mu\hat{A}_\nu - \partial_\nu\hat{A}_\mu$. The functions $Z(\phi)$, $\hat{Z}(\phi)$, and $V(\phi)$ that encode the non-perturbative features of our system are calibrated against lattice QCD data.

The magnetic field B breaks Lorentz invariance along the z-axis, leading to anisotropic pressure. Solving the bulk equations of motion (EoMs) allows us to extract thermodynamic quantities, such as the free energy density Ω, longitudinal pressure P_z, entropy density s, baryon density n_B, and magnetization M. For further details, see Supplementary Material [34]. This holographic approach provides a first-principles description of QCD dynamics under extreme conditions.

Neural ODEs—In the absence of a first-principle method to determine the coupling functions in our bottom-up model, we constrain this functional using available lattice QCD data—a challenge known as the inverse problem. As lattice QCD data at finite B and μ_B become more abundant, manually tuning control parameters becomes impractical. Instead of traditional neural networks that approximate solutions in a fixed finite-dimensional parameter space, our neural ODE approach systematically explores the infinite-dimensional parameter space of the coupling functions, achieving higher precision and accuracy.

In practice, we impose boundary conditions at both the ultraviolet (UV) boundary and the black hole event horizon. By solving the EoMs numerically, the neural ODE generates a trial equation of state that is iteratively optimized through backpropagation to reduce deviations from lattice QCD data. This process efficiently converges to an optimal magnetic coupling, providing a good agreement with lattice data and refining model predictions across unexplored magnetic fields and chemical potentials, see Fig. 1 for illustration. A detailed algorithmic breakdown of this methodology is included in the Supplementary Material [34]. More precisely, we construct a (2+1)-flavor holographic QCD model, using this neural ODE approach to achieve a precise fit with lattice QCD results [22]. A similar neural ODE-based method is applied to determine $Z(\phi)$ and $V(\phi)$ by matching to data at $B = 0$ [21, 38]. The resulting functional forms are benchmarked rigorously and agree with recent lattice simulations and experimental data [39, 40].

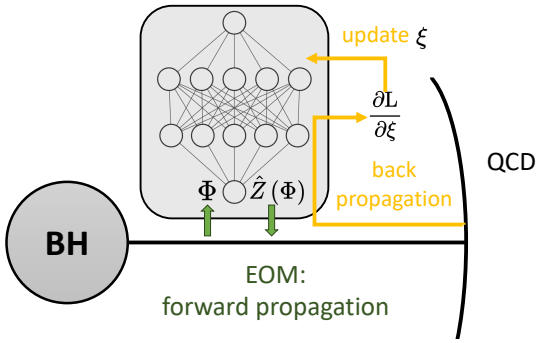

FIG. 1. Illustration of the neural ODE approach to the inverse problem of QCD phase diagram: The initial conditions for horizon are connected with boundary QCD by EOM. The function to be solved $\hat{Z}$ is used as the initialized neural network to enter the EOM solution. L is the loss function, which represents the gap between the model and lattice QCD. ξ represents all the parameters of the neural network $\hat{Z}$, which is solved by the gradient descent optimization method. The detailed calculation process of gradient $\frac{\partial L}{\partial \xi}$ is provided in the Supplementary Material [34]

Fig. 2 presents our holographic predictions for four independent thermodynamic quantities: magnetic susceptibility χ^B, magnetization M, entropy density s, and longitudinal pressure p_z, compared to lattice QCD data [22]. We find good agreement across the available magnetic fields, supporting our holographic model. This is the first holographic model to achieve good agreement with lattice data for magnetic fields up to $B = 0.6$ GeV^2. Further analysis is provided in the Supplementary Material, showing consistency with lattice QCD results [22].

QCD phase diagram—With the model fully established, we construct the QCD phase diagram at finite B, T, and μ_B by computing the free energy density Ω. The full phase diagram is depicted in Fig. 3. The light blue area denotes the first-order phase transition surface, dividing the quadrant into two parts: the high-temperature region corresponds to the quark-gluon plasma, while the low-temperature region corresponds to the hadron gas phase. The deep blue line in the diagram marks the location of CEP for various magnetic fields, where the first-order phase transition terminates and transitions into a smooth crossover at small chemical potentials. At $B = 0$, the phase diagram was presented in Fig. 3 of [39], where the first-order transition line ter-

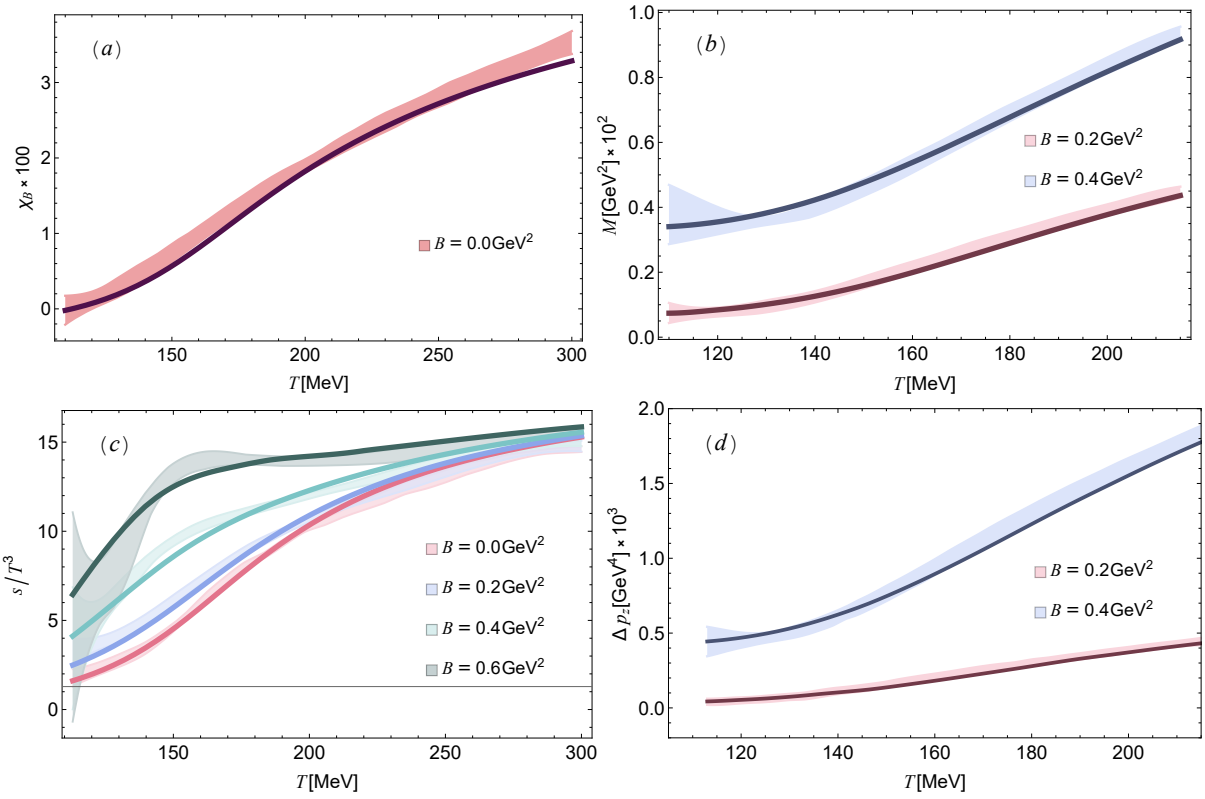

FIG. 2. Thermodynamic Quantities from Holographic QCD Model vs. Lattice Data. Temperature dependence of (a) magnetic susceptibility χ_B, (b) magnetization M, (c) entropy density s/T^3, and (d) longitudinal pressure $\Delta p_z = p_z|_B - p_z|_{B=0}$ across magnetic fields. Shaded regions show lattice QCD estimates [22]; solid lines indicate model predictions. Here, $e = 1$, giving $B = 1\,\text{GeV}^2 = 1.602 \times 10^{19}$ Gauss.

minates at ($T_C = 105\,\text{MeV}, \mu_C = 555\,\text{MeV}$). Similarly, the phase structure in the T-B plane at $\mu_B = 0$ reveals a line of first-order transitions ending at the CEP with ($T_C = 89.6\,\text{MeV}, B = 1.6\,\text{GeV}^2$), consistent with lattice QCD predictions [41].

Fig. 3 highlights the following three key observations [42].

1. As the magnetic field B increases up to $B = 1.618\,\text{GeV}^2$, the critical chemical potential μ_C at the CEP decreases, indicating that stronger magnetic fields shift the CEP to lower chemical potentials.

2. The critical temperature T_C at the CEP initially decreases with increasing B, reaching a minimum before increasing again. This turning point occurs around $T = 80\text{MeV}$, $B = 1.6 \sim 1.7\text{GeV}^2$, and $\mu_B = 0.2 \sim 0.28\text{GeV}$. This behavior suggests complicated effects in the presence of a background magnetic field. It could related to the inverse magnetic catalysis and magnetic catalysis reported in the literature.

3. At sufficiently strong magnetic field, multiple CEPs develop in the T-μ_B plane, as shown in Fig. 4. A first-order phase transition is observed for $0 < \mu_B < \mu_{C1}$ and $\mu_B > \mu_{C2}$, while a crossover occurs for $\mu_{C1} < \mu_B < \mu_{C2}$. As B increases, μ_{C1} and μ_{C2} converge to a single point. This reveals a rich phase structure in a strong magnetic field and warrants further experimental verification.

Critical exponents—Beyond mapping the phase diagram, we examine critical behavior near the CEPs via critical exponents. These exponents describe how thermodynamic quantities, such as susceptibility and specific heat, diverge near critical points, typically following power-law scaling. These exponents help identify the CEP's universality class and provide insights into QCD transitions under extreme conditions.

Four critical exponents can be directly extracted from the phase diagram of Fig. 3.

- **Critical exponent α:** The exponent α quantifies the power-law behavior of specific heat near a CEP along the axis defined as approaching the CEP along the tangent of the first-order line:

$$C_n = T\left(\frac{\partial s}{\partial T}\right)_{n_B,B} \sim |T - T_{\text{CEP}}|^{-\alpha}.$$

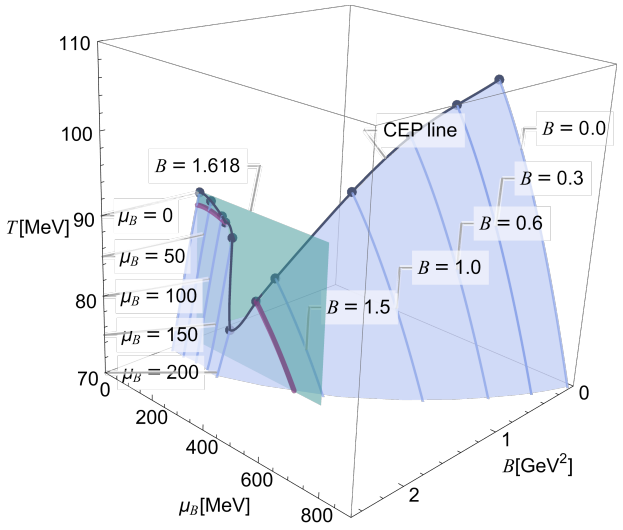

FIG. 3. QCD Phase Diagram at Finite Magnetic Field B. Phase structure in temperature T, baryon chemical potential μ_B, and magnetic field B from our holographic model. The light blue surface denotes the first-order transition boundary, separating the hadronic phase from the quark-gluon plasma. The dark blue line traces the CEP trajectory, marking where the first-order transition ends in a crossover.

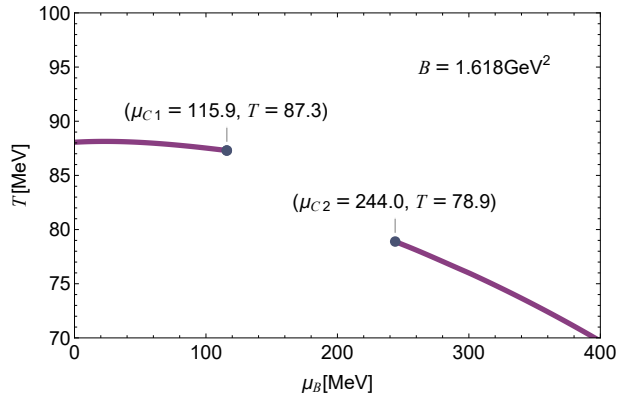

FIG. 4. QCD Phase Diagram in the T-μ_B Plane at $B = 1.618\,\mathrm{GeV}^2$. The purple line shows the first-order transition ending at the first critical endpoint (CEP) at $\mu_{C1} = 115.9\,\mathrm{MeV}$, where it transitions to a crossover. A second CEP appears at $\mu_{C2} = 224.0\,\mathrm{MeV}$, indicating an additional crossover at higher μ_B.

- **Critical exponent β:** It characterizes the discontinuity of entropy density s across the first-order line:

$$\Delta s = s_> - s_< \sim (T_{\mathrm{CEP}} - T)^{\beta},$$

where $s_>$ and $s_<$ represent the entropy densities in the high- and low-temperature phases, respectively.

- **Critical exponent γ:** It represents the power-law behavior of baryon susceptibility with the temperature near the CEP along the first-order axis:

$$\chi_2^B = \frac{1}{T^2}\left(\frac{\partial n_B}{\partial \mu_B}\right)_{T,B} \sim |T - T_{\mathrm{CEP}}|^{-\gamma}.$$

- **Critical exponent δ :** The definition of δ relies on the power-law relationship between entropy and chemical potential with $T = T_{\mathrm{CEP}}$ at the critical isotherm:

$$s - s_{\mathrm{CEP}} \sim |\mu_B - \mu_{B\mathrm{CEP}}|^{1/\delta},$$

where s_{CEP} is the entropy density at the CEP.

Table I presents the critical exponents for the CEP at three different magnetic field values, denoted by hQCD (I, II, III) [42]. The critical exponents satisfy the scaling relations $\alpha + 2\beta + \gamma = 2$ and $\alpha + \beta(1 + \delta) = 2$, ensuring the self-consistency of our results. Although close to mean-field values, these exponents show significant deviations depending on the CEP location, particularly as B increases. Such deviations highlight the features of our holographic QCD model, which cannot be attributed to large-N effects typical in conventional holographic duality, where mean-field behavior is expected. Based on 2+1-flavor lattice QCD data with $N_c = 3$, our model captures critical behavior distinct from mean-field theory, reinforcing its capability to describe non-mean-field dynamics. In the holographic 2-flavor model [43], the critical exponents match those of the quantum 3D Ising model, further emphasizing the distinct nature of our approach compared to traditional large-N QCD models.

	α	β	γ	δ
Experiment	0.110-0.116	0.316-0.327	1.23-1.25	4.6-4.9
3D Ising	0.110(5)	0.325±0.0015	1.2405±0.0015	4.82(4)
Mean field	0	1/2	1	3
DGR model	0	0.482	0.942	3.035
hQCD(I)	0.002296	0.485518	0.9558187	3.00993
hQCD(II)	0.001694	0.50373	0.91803	2.9455
hQCD(III)	0.00917	0.3944	0.98696	3.9878

TABLE I. Critical exponents from experiments in non-QCD fluids, the full quantum 3D Ising model, mean-field (van der Waals) theory, the DGR model [10], and our 2+1-flavor hQCD model. The hQCD (I, II, III) correspond to the critical exponents for $\mu_B = 554.66$ MeV, $B = 0$ (hQCD I), $\mu_B = 501.4$ MeV, $B = 0.3$ GeV^2 (hQCD II), and $\mu_B = 0$, $B = 1.6$ GeV^2 (hQCD III), respectively.

Conclusion– We have developed a novel neural ODE framework that solves the inverse problem of constructing a holographic QCD action from observational data. This framework results in the first holographic model capable of capturing key thermodynamic behaviors of hot and dense QCD at finite magnetic fields. Notably, the model reveals a rich phase structure in a strong magnetic field, including non-monotonic CEP temperature behavior (Fig. 3) and multiple CEPs in the T-μ_B plane

(Fig. 4), providing specific experimental markers for validation at future facilities like FAIR, JPARC-HI, and NICA [44]. Furthermore, we have determined critical exponents that depend on the location of CEPs, offering valuable insights for experimental studies in regions accessible to RHIC and LHC. Experimental observables, such as baryon number or magnetization fluctuations, could directly test these predictions in current experiments, e.g. RHIC [45], the STAR fixed target program (FXT), and future experiments [44].

Future research should extend the model to include isospin asymmetry, rotation effects, and real-time dynamics, thereby bridging gaps between theoretical predictions and experimental findings across energy scales. This includes incorporating isospin asymmetry, which is relevant for neutron stars, and rotational effects, which are critical for understanding dynamics in rapidly spinning neutron stars and heavy-ion collisions. Extending the model to non-equilibrium scenarios could also provide insights into the real-time dynamics of phase transitions, capturing rapid changes in temperature, density, and magnetic field during heavy-ion collisions. Exploring other bottom-up or top-down holographic models could help establish whether features like dual CEPs are universal in strongly coupled QCD-like theories or specific to our model. Applying our findings to neutron stars and early universe conditions, where understanding the equation of state for strongly interacting QCD matter under varying magnetic fields is crucial, presents another promising direction for future research.

Acknowledgements–We thank Heng-Tong Ding, Matti Järvinen, Elias Kiritsis, Zhibin Li, Yi-Bo Yang, Danning Li, Javier Subils, Ling-Xiao Wang, Shao-Jiang Wang, Yuan-Xu Wang, Yi Yang, and Peihung Yuan for stimulating discussions. This work is supported in part by the National Key Research and Development Program of China Grants No.2020YFC2201501 and No.2020YFC2201502, in part by the National Natural Science Foundation of China Grants No.12075101, No.12047569, No.12122513, No.12075298, No.11991052, No.12235016 and No.12047503. S.H. also would like to appreciate the financial support from the Max Planck Partner Group.

* cairg@itp.ac.cn,
hesong@jlu.edu.cn,
liliphy@itp.ac.cn

[1] P. Braun-Munzinger and J. Wambach, "The Phase Diagram of Strongly-Interacting Matter," Rev. Mod. Phys. **81** (2009), 1031-1050 [arXiv:0801.4256 [hep-ph]].

[2] O. Philipsen, "The QCD equation of state from the lattice," Prog. Part. Nucl. Phys. **70** (2013), 55-107 [arXiv:1207.5999 [hep-lat]].

[3] S. Gupta, X. Luo, B. Mohanty, H. G. Ritter and N. Xu, "Scale for the Phase Diagram of Quantum Chromodynamics," Science **332** (2011), 1525-1528 [arXiv:1105.3934 [hep-ph]].

[4] J. O. Andersen, W. R. Naylor and A. Tranberg, "Phase diagram of QCD in a magnetic field: A review," Rev. Mod. Phys. **88**, 025001 (2016) [arXiv:1411.7176 [hep-ph]].

[5] M. D'Elia, M. Mariti and F. Negro, "Susceptibility of the QCD vacuum to CP-odd electromagnetic background fields," Phys. Rev. Lett. **110**, no.8, 082002 (2013) [arXiv:1209.0722 [hep-lat]].

[6] T. Demircik, C. Ecker and M. Järvinen, "Dense and Hot QCD at Strong Coupling," Phys. Rev. X **12** (2022) no.4, 041012 [arXiv:2112.12157 [hep-ph]].

[7] Y. Chen, D. Li and M. Huang, "The dynamical holographic QCD method for hadron physics and QCD matter," Commun. Theor. Phys. **74** (2022) no.9, 097201 [arXiv:2206.00917 [hep-ph]].

[8] R. Rougemont, J. Grefa, M. Hippert, J. Noronha, J. Noronha-Hostler, I. Portillo and C. Ratti, "Hot QCD phase diagram from holographic Einstein–Maxwell–Dilaton models," Prog. Part. Nucl. Phys. **135** (2024), 104093 [arXiv:2307.03885 [nucl-th]].

[9] S. S. Gubser, A. Nellore, S. S. Pufu and F. D. Rocha, "Thermodynamics and bulk viscosity of approximate black hole duals to finite temperature quantum chromodynamics," Phys. Rev. Lett. **101** (2008), 131601 [arXiv:0804.1950 [hep-th]].

[10] O. DeWolfe, S. S. Gubser and C. Rosen, "A holographic critical point," Phys. Rev. D **83** (2011), 086005 [arXiv:1012.1864 [hep-th]].

[11] O. DeWolfe, S. S. Gubser and C. Rosen, "Dynamic critical phenomena at a holographic critical point," Phys. Rev. D **84** (2011), 126014 [arXiv:1108.2029 [hep-th]].

[12] U. Gursoy, M. Jarvinen and G. Nijs, "Holographic QCD in the Veneziano Limit at a Finite Magnetic Field and Chemical Potential," Phys. Rev. Lett. **120** (2018) no.24, 242002 [arXiv:1707.00872 [hep-th]].

[13] J. Grefa, J. Noronha, J. Noronha-Hostler, I. Portillo, C. Ratti and R. Rougemont, "Hot and dense quark-gluon plasma thermodynamics from holographic black holes," Phys. Rev. D **104** (2021) no.3, 034002 [arXiv:2102.12042 [nucl-th]].

[14] S. He, S. Y. Wu, Y. Yang and P. H. Yuan, "Phase Structure in a Dynamical Soft-Wall Holographic QCD Model," JHEP **04** (2013), 093 [arXiv:1301.0385 [hep-th]].

[15] T. Alho, M. Järvinen, K. Kajantie, E. Kiritsis, C. Rosen and K. Tuominen, "A holographic model for QCD in the Veneziano limit at finite temperature and density," JHEP **04** (2014), 124 [erratum: JHEP **02** (2015), 033] [arXiv:1312.5199 [hep-ph]].

[16] J. Knaute, R. Yaresko and B. Kämpfer, "Holographic QCD phase diagram with critical point from Einstein–Maxwell-dilaton dynamics," Phys. Lett. B **778** (2018), 419-425 [arXiv:1702.06731 [hep-ph]].

[17] R. Critelli, J. Noronha, J. Noronha-Hostler, I. Portillo, C. Ratti and R. Rougemont, "Critical point in the phase diagram of primordial quark-gluon matter from black hole physics," Phys. Rev. D **96** (2017) no.9, 096026 [arXiv:1706.00455 [nucl-th]].

[18] Y. Yang and P. H. Yuan, 'QCD Phase Diagram by Holography," [arXiv:2011.11941 [hep-th]].

[19] R. G. Cai, S. He and D. Li, "A hQCD model and its phase diagram in Einstein-Maxwell-Dilaton system," JHEP **03**

(2012), 033 [arXiv:1201.0820 [hep-th]].

[20] S. I. Finazzo, R. Critelli, R. Rougemont and J. Noronha, "Momentum transport in strongly coupled anisotropic plasmas in the presence of strong magnetic fields," Phys. Rev. D **94** (2016) no.5, 054020 [arXiv:1605.06061 [hep-ph]].

[21] A. Bazavov *et al.* [HotQCD], "Equation of state in (2+1)-flavor QCD," Phys. Rev. D **90** (2014), 094503 [arXiv:1407.6387 [hep-lat]].

[22] G. S. Bali, F. Bruckmann, G. Endrődi, S. D. Katz and A. Schäfer, "The QCD equation of state in background magnetic fields," JHEP **08**, 177 (2014) [arXiv:1406.0269 [hep-lat]].

[23] K. Hashimoto, S. Sugishita, A. Tanaka and A. Tomiya, "Deep Learning and Holographic QCD," Phys. Rev. D **98**, no.10, 106014 (2018) [arXiv:1809.10536 [hep-th]].

[24] T. Akutagawa, K. Hashimoto and T. Sumimoto, "Deep Learning and AdS/QCD," Phys. Rev. D **102**, no.2, 026020 (2020) [arXiv:2005.02636 [hep-th]].

[25] K. Hashimoto, H. Y. Hu and Y. Z. You, "Neural ordinary differential equation and holographic quantum chromodynamics," Mach. Learn. Sci. Tech. **2**, no.3, 035011 (2021) [arXiv:2006.00712 [hep-th]].

[26] K. Hashimoto, K. Ohashi and T. Sumimoto, "Deriving the dilaton potential in improved holographic QCD from the chiral condensate," PTEP **2023**, no.3, 033B01 (2023) [arXiv:2209.04638 [hep-th]].

[27] X. Chen and M. Huang, "Machine learning holographic black hole from lattice QCD equation of state," Phys. Rev. D **109** (2024) no.5, L051902 [arXiv:2401.06417 [hep-ph]].

[28] Y. Bea, R. Jimenez, D. Mateos, S. Liu, P. Protopapas, P. Tarancón-Álvarez and P. Tejerina-Pérez, "Gravitational duals from equations of state," JHEP **07**, 087 (2024) [arXiv:2403.14763 [hep-th]].

[29] In most studies, e.g. [13, 16–18], the thermodynamic variables were obtained by integrating the standard first law of thermodynamics, whose validity is still under investigation for AdS black holes with scalar hair [30–33].

[30] L. Li, "On Thermodynamics of AdS Black Holes with Scalar Hair," Phys. Lett. B **815** (2021), 136123 [arXiv:2008.05597 [gr-qc]].

[31] T. Hertog and G. T. Horowitz, "Designer gravity and field theory effective potentials," Phys. Rev. Lett. **94**, 221301 (2005) [arXiv:hep-th/0412169 [hep-th]].

[32] A. Anabalon, D. Astefanesei, D. Choque and C. Martinez, "Trace Anomaly and Counterterms in Designer Gravity," JHEP **03**, 117 (2016) [arXiv:1511.08759 [hep-th]].

[33] H. Lu, C. N. Pope and Q. Wen, "Thermodynamics of AdS Black Holes in Einstein-Scalar Gravity," JHEP **03**, 165 (2015) [arXiv:1408.1514 [hep-th]].

[34] The Supplemental Material provides detailed discussions on the equations of motion, definitions of thermodynamic quantities, and the neural ODE methodology. It also includes references [35–37] not cited in the main text.

[35] Kingma, D. P., Ba, J., "Adam: A method for stochastic optimization," [arXiv:1412.6980].

[36] R. T. Q. Chen, Y. Rubanova, J. Bettencourt, and D. K. Duvenaud, "Neural Ordinary Differential Equations," Advances in Neural Information Processing Systems, vol. 31, 2018.

[37] S. Shi, L. Wang and K. Zhou, "Rethinking the ill-posedness of the spectral function reconstruction — Why is it fundamentally hard and how Artificial Neural Networks can help," Comput. Phys. Commun. **282**, 108547 (2023) [arXiv:2201.02564 [hep-ph]].

[38] S. Borsányi, Z. Fodor, J. N. Guenther, R. Kara, S. D. Katz, P. Parotto, A. Pásztor, C. Ratti and K. K. Szabó, "Lattice QCD equation of state at finite chemical potential from an alternative expansion scheme," Phys. Rev. Lett. **126** (2021) no.23, 232001 [arXiv:2102.06660 [hep-lat]].

[39] R. G. Cai, S. He, L. Li and Y. X. Wang, "Probing QCD critical point and induced gravitational wave by black hole physics," Phys. Rev. D **106** (2022) no.12, L121902 [arXiv:2201.02004 [hep-th]].

[40] Z. Li, J. Liang, S. He and L. Li, "Holographic study of higher-order baryon number susceptibilities at finite temperature and density," Phys. Rev. D **108**, no.4, 046008 (2023) [arXiv:2305.13874 [hep-ph]].

[41] F. Cuteri, "QCD thermodynamics: an overview of recent progress," PoS **LATTICE2022** (2023), 243

[42] As the quantitative results significantly depend on computational power, we plan to present more detailed phase structures and additional findings on the critical exponents in the forthcoming version.

[43] Y. Q. Zhao, S. He, D. Hou, L. Li and Z. Li, "Phase structure and critical phenomena in two-flavor QCD by holography," Phys. Rev. D **109** (2024) no.8, 086015 [arXiv:2310.13432 [hep-ph]].

[44] K. Fukushima, B. Mohanty and N. Xu, "Little-Bang and Femto-Nova in Nucleus-Nucleus Collisions," AAPPS Bull. **31**, 1 (2021) [arXiv:2009.03006 [hep-ph]].

[45] J. Adam *et al.* [STAR], "Nonmonotonic Energy Dependence of Net-Proton Number Fluctuations," Phys. Rev. Lett. **126**, no.9, 092301 (2021) [arXiv:2001.02852 [nucl-ex]].